Journal Pre-proof

Acidichromic Organic Crystals with Manifold Mechanical Deformations for Reconfigurable Flexible Optical Tuner

Xiuhong Pan, Linfeng Lan, Qi Di, Xuesong Yang, Hongyu Zhang

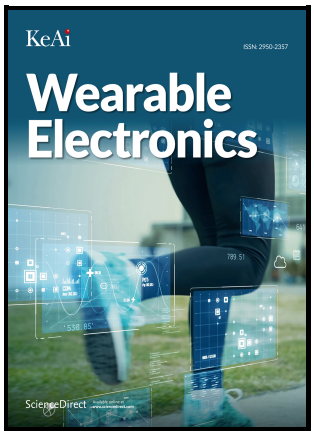

PII: S2950-2357(24)00007-6

DOI: https://doi.org/10.1016/j.wees.2024.05.003

Reference: WEES6

To appear in: *Wearable Electronics*

Received date: 16 March 2024
Revised date: 10 April 2024
Accepted date: 8 May 2024

Please cite this article as: Xiuhong Pan, Linfeng Lan, Qi Di, Xuesong Yang and Hongyu Zhang, Acidichromic Organic Crystals with Manifold Mechanical Deformations for Reconfigurable Flexible Optical Tuner, *Wearable Electronics,* (2024) doi:https://doi.org/10.1016/j.wees.2024.05.003

Acidichromic Organic Crystals with Manifold Mechanical Deformations for Reconfigurable Flexible Optical Tuner

Xiuhong Pan, Linfeng Lan, Qi Di, Xuesong Yang, and Hongyu Zhang*
State Key Laboratory of Supramolecular Structure and Materials, College of Chemistry, Jilin University, Changchun 130012, Jilin Province, China
* Corresponding Author: hongyuzhang@jlu.edu.cn

ABSTRACT: Acicular organic crystals with micro- or centimeter scale in length have been widely employed as media for transducing self-emitted or inputted optical signals, i.e., active or passive optical waveguides. Combining the emerging dynamic adaptability of crystals with optical waveguides, provides an unprecedented opportunity to development of crystal-based organic flexible optoelectronics devices. Here, we report a Schiff base crystal that combines two unique features of integrated elastic-bending, plastic-twisting, acid-bending deformations and protonation-induced crystal acidichromism. The emission color of a single crystal can be selectively and reversibly regulated at different locations between green (554 nm) and deep red (659 nm) by protonic acid vapor fuming, producing various block heterojunction structures easily identified by color and emission. In addition, the flexible heterojunction structures can be reconfigured by a quickly repeated erasing-writing process based on reversible protonation-deprotonation. Making full use of the integrated flexibilities, acidichromic and optical waveguides properties of crystals, a flexible optical crystalline tuner with a wide range of output signals that can be adjusted flexibly was further constructed. These results not only demonstrate that reconfigurable optical structures can be designed using organic crystals, but also open prospects for the application of flexible organic crystals in lightweight, wearable electronic devices.

KEYWORDS: organic crystals, elastic-bending, plastic-twisting, reconfigurable, acidichromic, optical waveguides

GRAPHICAL ABSTRACT

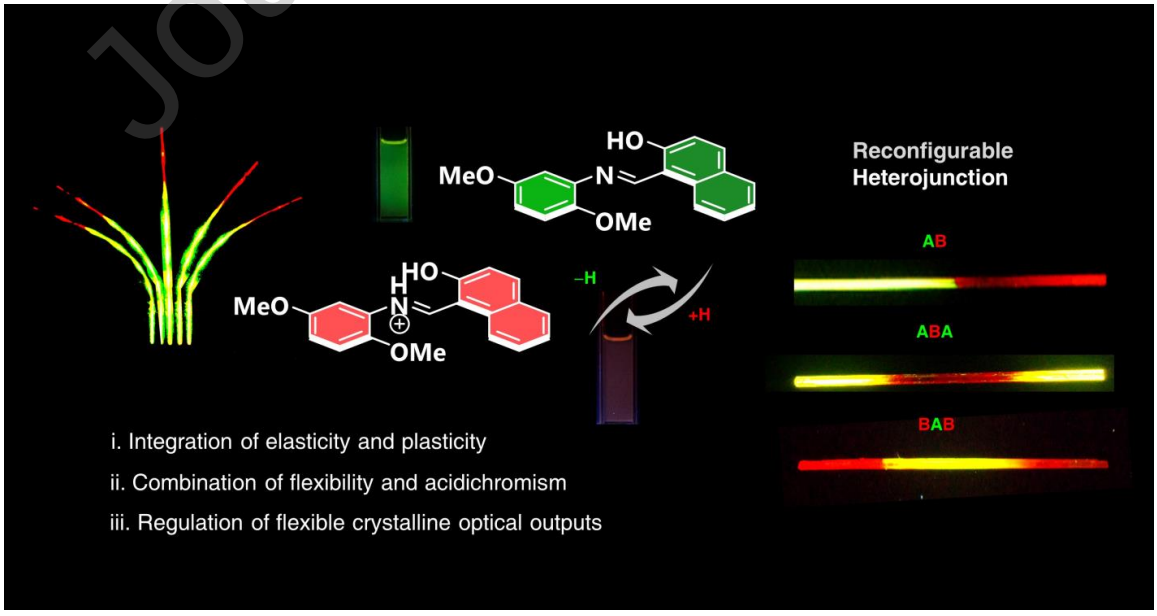

HIGHLIGHTS

- Elastic-bending and plastic-twisting properties in organic crystals
- Acid-bending deformations induced by protonation
- Protonation-induced acidichromism for reversible emission color control
- Reconfigurable optical waveguides enabling adaptable signal outputs

1. Introduction

In recent years, wearable electronic devices have received considerable attention, permeating every aspect of our daily lives and stimulating interest in futuristic electronics.[1,2] Thus, flexible materials that can be bent or folded are desperately needed, given the increasing demand for wearable electronics.[1-4] Organic flexible crystal materials have characteristic advantages of high crystallinity, light-weight, long-range ordered molecular packing structure, and most importantly anisotropic physical properties, and are expected to be suitable for the field of flexible electronics.[5-8] Regardless of which stimulus the crystals are induced by (force,[9,10] chemical vapors,[11,12] light,[13,14] heat[15]), their macroscopic dynamic effects can be expressed as bending,[16-18] curling,[19,20] twisting,[21-23] jumping.[15,24,25]A large number of dynamic and mechanically compliant organic crystals have quickly shaped a novel hot frontier in material science.[10,26,27] The anisotropic nature of organic crystals enables the possible integration of elasticity and plasticity[28,29], which would enrich the complexation of deformations and applications as well as reduce the broken risk of crystals, however, this remains a formidable challenge.

Molecular crystals are generally brittle and are considered to lack the flexibility required for current applications developed by more easily processed organic polymers or elastomers. However, emerging research into the mechanical properties of flexible organic molecular crystals has breathed new life into their potential applications.[30-34] For instance, passive and/or active crystalline optical waveguides as well as amplified spontaneous emissions[32-34] have been achieved for elastically or plastically bendable organic crystals. Moreover, light polarization rotation, a well-known function of liquid crystals, has been recently realized through manually twisting organic crystals followed by recording the crystalline optical waveguides.[21,34] Considering the great potential of flexible crystal optical waveguides in integrated micro optoelectronics, the modulation of optical output is very significant. Chemical structure modification is the general strategy to implement flexible crystalline optical waveguides with different outputs, however, it requires complex syntheses and laborious purifications. Crystal engineering, as an alternative protocol, has also been used to modulate the flexible crystal waveguide output. Unfortunately, it is difficult to endow the required flexibility and large emission differences to polymorphs.

Aiming at combining mechanical flexibility and color modulation capability into an organic crystal, we choose a Schiff base derivative based on the considerations of 1) Schiff base derivatives have been widely employed to design mechanically deformable crystals[21,35-37] and 2) the electronegative nitrogen atom has the ability to react with proton and produce the corresponding cation species with totally different electronic structures (optical properties).[12] These two stimuli-responsive properties are thus expected to be merged in a Schiff base crystal. In this work, we report an organic crystal possessing independently controllable elasticity (bending) and plasticity (twisting) that is compatible with acidichromic behaviors based on a Schiff base (E)-1-(((2,5-dimethoxyphenyl)imino)methyl)naphthalen-2-ol (**1**). Centimeter-scale crystals **1** presented in this study are capable of responding to transversal stress and shearing force with deformations of elastically bending and plastically twisting, respectively, and even undergo permanent deformation under acid vapor stimulation. Moreover, crystalline samples of compound **1** display acidichromsim with emission

color change from green to deep red when fuming in volatile protonic acids such as hydrochloric acid (HCl) or trifluoroacetic acid (TFA) while retaining their bendable and twistable flexibilities. Photophysical and mechanical properties, crystal structures, and various acidichromic behaviours have been well investigated and discussed. Finally, a flexible heterogeneous structure whose output signal can be flexibly modulated was successfully prepared based on the above characteristics and the optical waveguide properties of crystal **1**. Leveraging the crystal's mechanical flexibility and acid-induced color modulation, active crystalline optical waveguides can be constructed. These waveguides offer high transduce-pathway deformability and wide-range output tunability, which could be advantageous for integrated micro optoelectronic applications. The crystal's multifaceted properties open up possibilities for various applications in flexible optics, reconfigurable electronics, and optoelectronic devices.

2. Results and Discussion

2.1 Photophysical properties

Compound **1** (Figure 1a) is synthesized through a simple one-step reaction and purified by column to yellow crystalline solids with a high yield (86.2%). Solution diffusion of hexane into dichloromethane (DCM) solution of **1** (0.1 M) in a beaker produced slender crystals with lengths up to 5.0 cm (Supporting Information Figure S1). As shown in Figure 1b, the color and emission of DCM solution **1** change dramatically upon adding HCl or TFA acid, and the formed protonated complex is defined as **1@H**. The crystalline solids **1** also show acidichromism upon fuming in HCl or TFA vapors. To further confirm the acidichromic mechanism, single crystals of the protonated complex (defined as **1•H**, Supporting Information Figure S2) have been successfully obtained by solvent diffusion approach with the additive of TFA acid. The attempt towards **1@H** containing HCl for single crystal X-ray diffraction failed due to its low degree and uneven distribution of protonation. A comparison of ^{1}H NMR spectra among **1**, **1@H** and **1•H** in deuterated dimethylsulfoxide demonstrates that there exists a dynamic equilibrium between protonation and deprotonation in solution (Figure 1b). Crystals **1•H** show a greater proportion of protonated molecules than fumed sample **1@H**, indicating that partial protonation takes place upon fuming the crystalline solids **1**.

UV-vis absorption and emission spectra of **1**, **1@H**, and **1•H** were recorded to investigate the variation of the fluorescence color change (Figure 1c, d). Compared with **1**, the protonated species **1@H** and **1•H** show longer wavelength absorption with an additional band in the range from 510 to 540 nm. Compound **1** displays green fluorescence peaking at 518 nm in DCM solution. Interestingly, **1@H** and **1•H** show orange-red fluorescence in DCM solution with emission peaks at 610 and 617 nm, which is red-shifted by 92 and 99 nm, respectively, demonstrating that the protonation significantly affects the electronic structures of compound **1**. The optical properties of **1**, **1@H**, and **1•H** solids are similar to those of solution samples. As shown in Figure 1e, the absorption bands of **1@H** and **1•H** are obviously red-shifted by about 60 nm compared with **1**. Crystals **1** display green fluorescence with an emission maximum at 540 nm, while crystals **1@H** and **1•H** show deep-red emission at 663 and 659 nm which are significantly red-shifted by 123 and 119 nm, respectively (Figure 1f). In this sense, the fluorescence of crystalline solids **1** can be conveniently regulated with a huge difference by protonic acid fuming. Theoretical calculations have been performed on both the neutral and cationic structures to disclose the electronic structures and energy levels. As shown in Supporting Information Figure S3, the highest occupied molecular orbital (HOMO) of **1** shows that the electron density has distribution on the entire molecule, and the electron density of the lowest unoccupied molecular orbital (LUMO) is distributed on naphthalene unit and C–N moiety. Differently, the distribution of HOMO and LOMO of the cationic species are separated, suggesting an intramolecular

charge transfer (ICT) character. The resultant energy gap between HOMO and LUMO of the neutral and cationic structures is calculated to be 3.275 eV and 2.589 eV, respectively, which corresponds to absorption at a wavelength of 380nm and 479 nm of **1**, **1@H** and **1•H**.

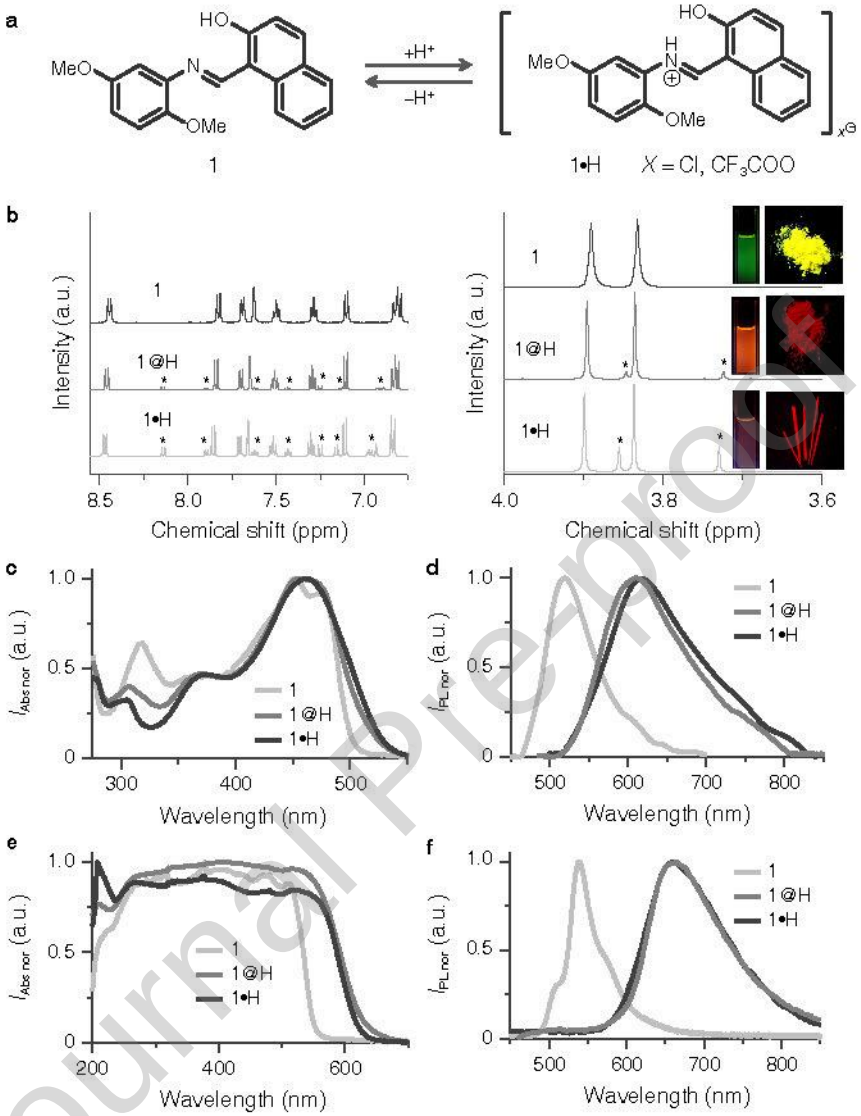

Figure 1 | (a) Protonated and deprotonated structure of compound **1**. (b) ^{1}H NMR spectra of **1**, **1@H**, and **1•H** (stars indicate the protonated molecules) and pictures of DCM solution and solid samples of **1**, **1@H**, and **1•H** under UV light. (c–f) Absorption (c) and emission (d) spectra of DCM solution samples of **1**, **1@H**, and **1•H**, and absorption (e) and emission (f) spectra of solid samples of **1**, **1@H**, and **1•H**.

2.2 Acidichromic behaviors

The acid-chromic property of single crystals **1** was investigated in detail and a series of reconfigurable heterostructures were prepared. Single crystals **1** were placed in a petri dish, in which a couple of cotton balls were placed close to the crystalline samples. After a few drops of concentrated HCl acid were added to the cotton balls, the color and emission of crystals changed from green to red within 1 minute (Figure 2a and Movie S1). The acidichromism phenomenon was analyzed in situ by recording the time-dependent emission spectra. Then, by controlling the amount of hydrochloric acid dripped onto the cotton, acid concentrations within the confined space was 0.0064 mol / L, 0.0127 mol / L, and 0.0255 mol / L,

respectively, to further the time required for crystal acid discoloration and the changes of fluorescence wavelength under different acid concentrations. The fluorescence changes of the three acid concentrations are basically the same, indicating that the acid concentration has little effect on the degree of protonation (Supporting Information Figure S4). In addition, the time required for acid discoloration decreases as the acid concentration increases, indicating that the high acid concentration is conducive to accelerating the protonation process. As shown in Figure 2e, the fluorescence of crystal **1** gradually red-shifted from 544 nm to 658 nm about 30 s, covering green, yellow, orange, red and deep red emissions. A comparison of powder X-ray diffraction patterns between crystal **1** and the fumed sample **1@H** verifies that only superficial molecules are protonated (Supporting Information Figure S5). The protonation degree (20.31 – 26.21%) has been briefly evaluated by calculating the weight of **1** and **1@H** (Supporting Information Table S1) after fuming crystalline powders with HCl vapor for 24 h. Notably, when the relevant **1@H** was taken out from the petri dish to air, deprotonation took place accompanied by recovery of fluorescence, indicating that this was a reversible process. The deprotonation is rather slow (Figure 2a, f) and heating will accelerate this process (Supporting Information Figure S6 and Movie S2). **1@H** sample nearly recovered to the original state after standing in the air for about 9 hours, while the fluorescence of the original can be quickly restored when placed at 60 °C about 30 s. Based on this sensitive and easy access approach as well as the long crystal length, selective protonation of different parts of a single crystal **1** to construct **AB** type heterojunction structures (defined as **1//1@H**) with high-contrast of emission color was realized. As shown in Figure 2b and 2c, a straight or a twisted (*vide infra*) crystal **1** was step-wise protonated to form heterojunction structures **1//1@H** with varied length ratios. The fluorescence can also be precisely regulated by controlling the acid-fuming time (Figure 2d, e). Due to the reversible protonation-deprotonation process, the fabrication of heterojunction structures is reconfigurable. A 1.5 cm crystal **1** was chosen for this purpose, and the setup for this partly protonation is represented in Supporting Information Figure S7. Two-fifths in length of the crystal was firstly fumed in HCl vapor for about 1 min, and the generated red emissive **1@H** can be erased by standing in the air at 60 °C within 30 s (Figure 2g). Similarly, under the same conditions, we could perform the repeated fumed and erased process in different proportions (30% and 70%) for the crystal. Other heterojunction structures such as **1//1@H//1 (ABA)** and **1@H//1//1@H (BAB)** can be also easily prepared by a similar procedure (Figure 2h). We confirm that more complicated heterojunction structures can also be fabricated based on the approach presented in this work.

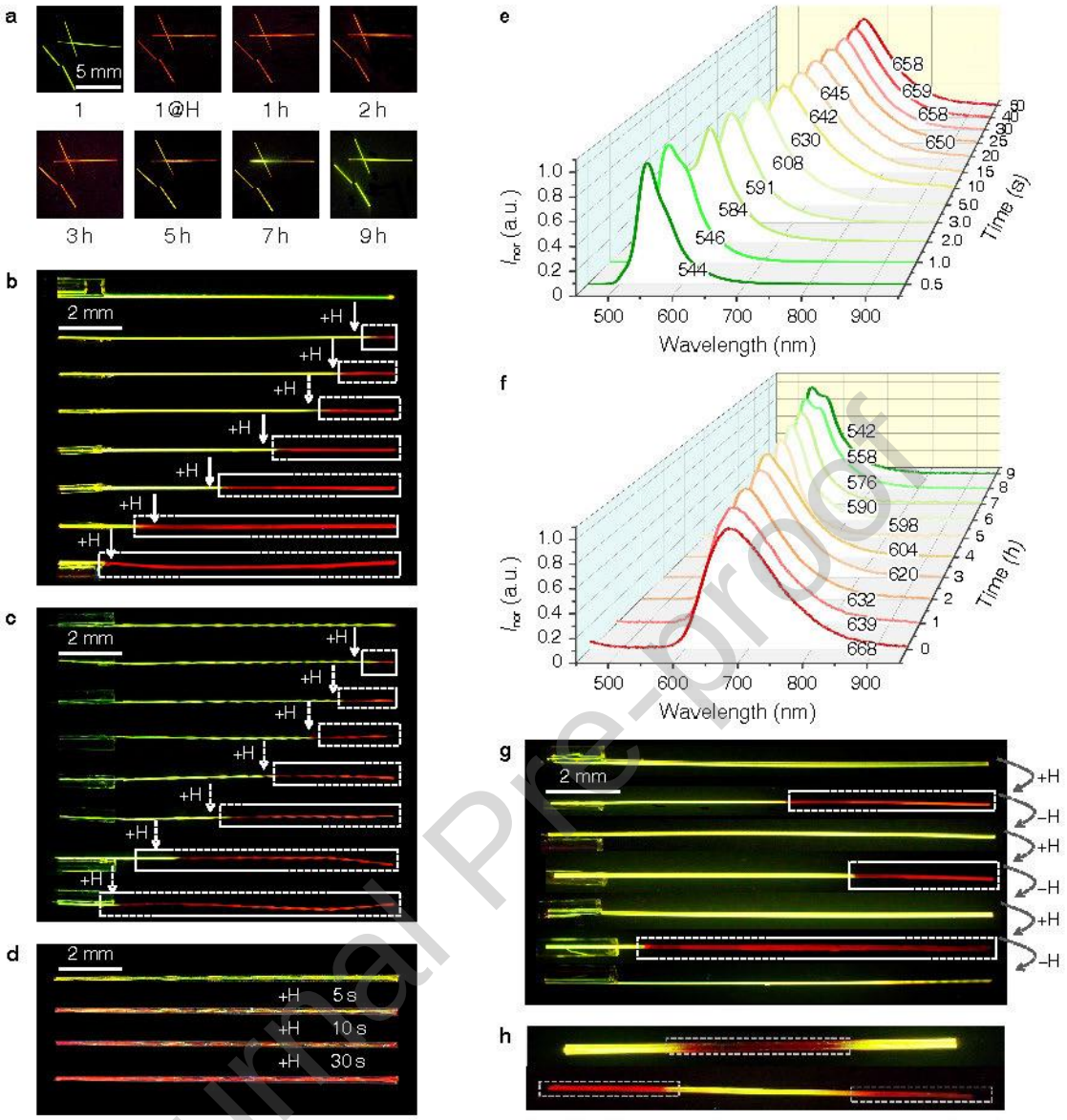

Figure 2 | (a, b) Photographic images of **1**, **1@H** and the recovering processes of the protonated crystals (a), step-wise protonation of a straight crystal **1** (b). (c, d) Step-wise protonation of a twisted crystal **1** (c), acid-fuming time-dependent protonation of a twisted crystal **1** (d). (e, f) Emission spectra of time-dependent protonation of crystal **1** (e), emission spectra of time-dependent deprotonation of **1@H** (f). (g, h) Reconfigurable protonation of a straight crystal **1** (g), and **ABA** and **BAB** heterojunction structures by selectively protonating (h). All dash line boxes represent protonated areas.

2.3 Mechanical properties

Subsequently, the mechanical properties of those different forms of crystals **1** including elastic-bending, plastic-twisting and even acid-bending were further evaluated. As shown in Figures 3a, when one tip of a crystal **1** or heterojunction **1//1@H** was fixed on a capillary, it can be elastically bent upon loading stress along the wide face (001). After releasing stress, it immediately returns to its original state. The bending-relaxing process could be repeated many times without obvious defects or fractures as demonstrated by the scanning electron microscopy (SEM) images (Figure 3b). AFM images further show that the surface roughness of the crystal increases to a certain extent after acid fumigation (Supporting Information Figure

S8). In addition, twisting the crystals by applying reverse torsion forces at two tips of a crystal **1** or **1@H**, right-handed or left-handed helical structures with pitch lengths of 0.7 – 1.0 and 1.0 – 1.5 mm, respectively, was obtained (Figure 3c, d and Supporting Information Figure S9). Notable, the twisted structures of **1** still retain smooth crystal surfaces (Figure 3f) and elastic-bending capability (Figure 3e, f). Thus, the integration of elasticity and plasticity in one heterostructure crystal was realized, and these two distinct deformations were independently controllable. In addition, similar to the previously reported compounds,[11,12] the finer crystals **1** (width: 30 – 60 μm, thickness: 20 – 40 μm) exhibited chemical bending during HCl vapor fumigation (Figure 3g and Supporting Information Figure S10). To confirm the mechanical elasticity of crystals **1** and **1@H**, three-point bending experiments were performed on crystals **1** and **1@H** (Figure 3h and Supporting Information Figure S11). The linear stress-strain curves of **1** and **1@H** shown in Figure 3i indeed confirm their elastic nature. The elastic modulus of **1@H** (1.71 GPa) increases to a certain degree compared with that of **1** (1.67 GPa), probably due to fuming-caused defects as implied by the SEM image (Figure 3f). Notably, crystals **1•H** also exhibit elasticity with a slightly larger elastic modulus (2.00 GPa) than **1@H** (Figure 3h and Supporting Information Figure S12). From multiple measurements, average Young modulus and hardness of crystal **1** was estimated to be 1.5 GPa and 0.03 GPa, respectively, indicating that crystals **1** are quite soft (Supporting Information Figure S13). The stability of stimulus-responsive materials is also significant. Therefore, we took a crystal **1** and repeat the reversible acid response process several times and leave it for a week under ambient temperature. The crystal was still able to bend repeatedly, and three-point bending experiment was further performed (Supporting Information Figure S14). The elastic modulus and optical loss coefficient of the sample are similar to that of the original crystal, indicating excellent robustness. The results support the general point that Schiff base compounds are preeminent candidates for constructing mechanically compliant crystals.

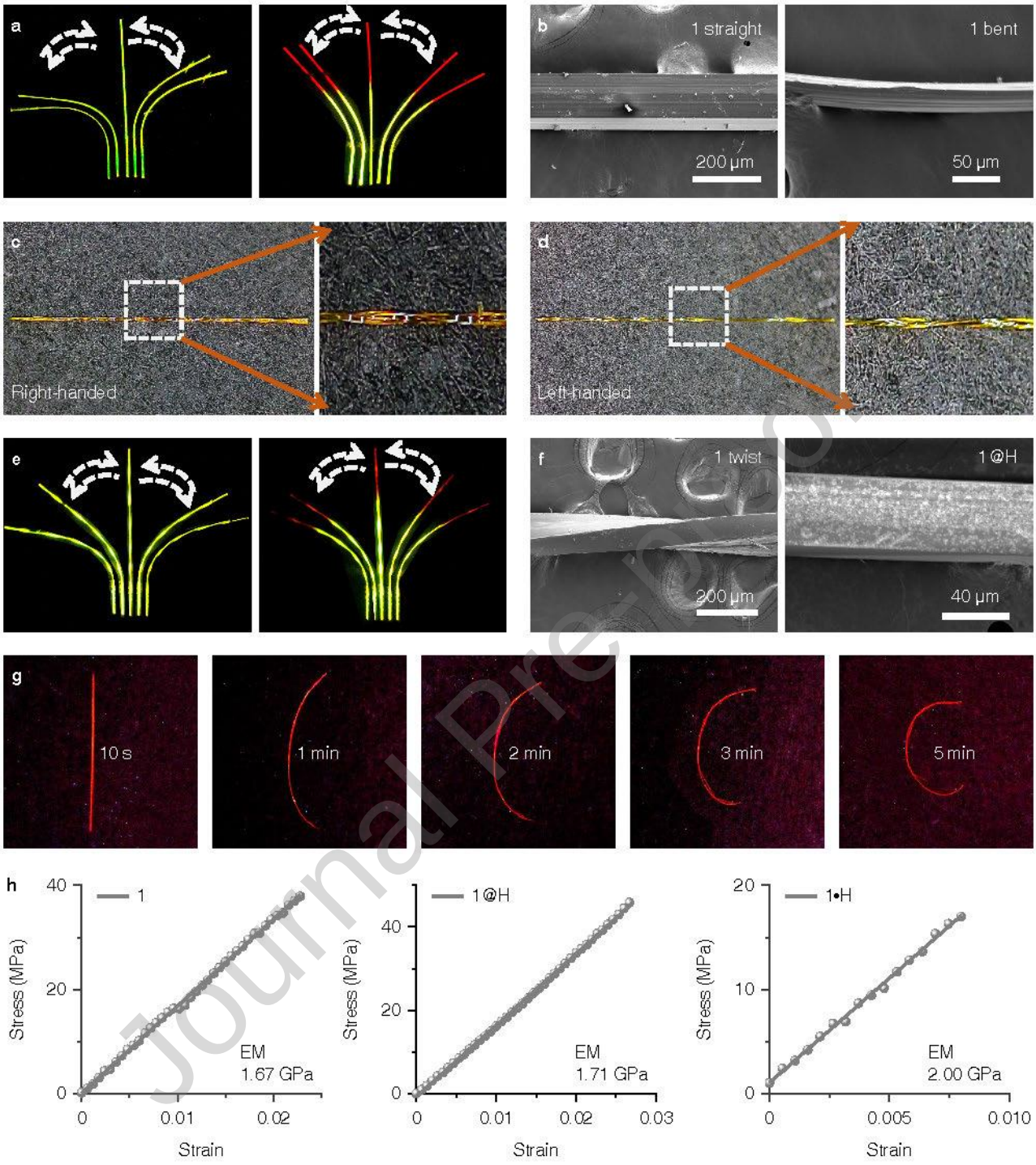

Figure 3 | (a) Elastically bending of a neutral (left) and partly protonated (right) crystal **1**. (b) SEM images of a straight, bent crystal **1**. (c, d) Right-handed (c) and left-handed (d) plastically twisting of a crystal **1**. (e) Elastically bending of a neutral and twisted (left) and partly protonated and twisted (right) crystal **1**. (f) SEM images of a twisted and acid-fumed crystal **1**. (g) Fuming-induced bending of crystal **1**. (h) The strain-stress curves of crystals **1**, **1@H**, and **1•H**.

2.4 Crystal structures

Single crystal X-ray diffractions have been carried out on **1** and **1•H** to provide insights into the acidichromsim and the independent yet integrated elastic-bending and plastic-twisting deformations

(Supporting Information Table S2).[38] **1** crystallized in the orthorhombic system, $P2_12_12_1$ space group, and there is one individual molecule in the unit cell. **1•H** crystallized in the monoclinic system and $P2_1/c$ space group, and one molecule connected with two TFA molecules of which one serves as the proton donor and the other as the solvent (Supporting Information Figure S15). According to the crystal structure shown in Figures 4a and 4c, we note that ground state intramolecular proton-transfer (GSIPT) takes place (Supporting Information Scheme S1) for this Schiff base compound. The active hydrogen atom is reasonably added to the N atom based on residual peak hydrogenation, as a result, the covalent bonds $C_1{-}O_1$ and $C_{10}{-}C_{11}$ are significantly shortened in crystal **1** compared with those in **1•H**, which is indicative of a double bond character (Figure 4a, c). In **1•H**, the carbonyl moiety is protonated, which makes the π-system has a positive charge. In this case, the methoxyphenyl group serves as an electron donor whereas the other part as an electron acceptor. This strong ICT character is an important factor leading to acidichromism. In addition, the individual molecule in **1** takes a rather planar structure due to the efficient π-conjugation and intrinsic intramolecular hydrogen bond (H···O distance: 1.692 Å). Infinite column structures are formed along the crystal growth direction [100] by π···π interactions (3.319 – 3.343 Å) with a very short vertical distance of 2.959 Å. These columns are linked through intermolecular hydrogen bonds C–H···O with a H···O distance of 2.468 Å, generating a layer structure in the (001) plane (Figure 4b and Supporting Information Figure S16). Along the crystallographic [001] direction, the columns are connected by C–H···π interactions with a vertical distance of 2.736 Å. As a result, the bending plane (001) formed (Figure 4b), as determined by face indexing (Supporting Information Figure S17).

When the wide face (001) is loading external stress, the bending plane undergoes expansion in the outer arc enlarging π···π distance and contraction in the inner arc by shortening π···π distance, accompanied by slight molecular rotations to fit the changes in curvature at the macro level of the curved crystal. When the stress is released, the molecule easily returns to its original position, thus returning to a straight state. At the same time, the hydrogen bonds between the molecular layers buffer and dissipate partial stress, preventing the molecular layers from misalignment. As for the twisting deformation, the shearing force is mainly tangentially distributed on the (100) plane in which the columns are linked by C–H···π and C–H···O intermolecular interactions. Weak interactions involve two molecular sliding directions (Figure 4d) and facilitate slippage of the adjacent molecule columns, ultimately resulting in pronounced plastic twisting. When one straight crystal is twisted into a helical structure, the weak intermolecular interactions may break and some new interactions reform. The π-packing plane of the molecule slides and rotates around the central axis of the crystal to varying degrees to accommodate the torsional deformation. To visualize intermolecular interactions and further illustrate our hypothesis, the interaction energy frameworks of crystal **1** are analyzed by the CrystalExplorer software using the B_3LYP hybrid functional with 6–31G (*d*, *p*) basis set, where semiempirical dispersion is included by using the D_2 version of Grimme's dispersion.[39] In (010) and (001) planes, the thick blue cylinders with the largest total energy of –59.2 kJ/mol reflect the strongest interactions contributed by the π-stacked molecular columns that are responsible for layer contraction and expansion (Figure 4e). Other thinner cylinders perpendicular to the thicker ones with small total energies (*e.g.*, –14.6 kJ/mol) represent weak intermolecular interactions which promote short-range slippages thereby reducing the crystal brittleness. In the (100) plane, several thin cylinders, representing weak intermolecular interactions between π-stacked columns, are crosswise arranged and form networks, which indicates torsion energy dissipates pathways when twisting a crystal.

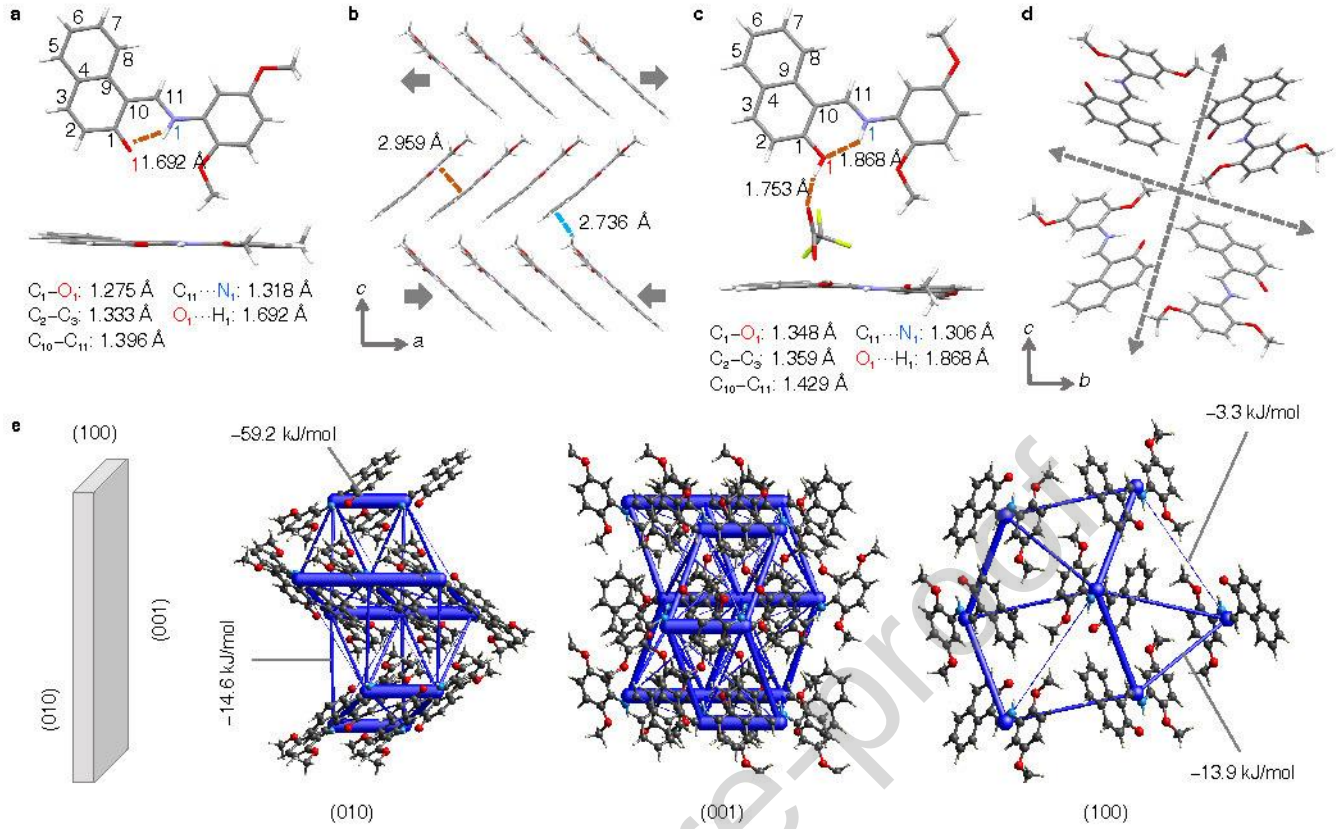

Figure 4 | (a) Molecular structures with some key covalent bond lengths and the intramolecular hydrogen bond in **1**. (b) Molecular packing structure view down (010) plane in crystal **1**.(c) Molecular structures with some key covalent bond lengths and the intramolecular hydrogen bond in **1•H**. (d) Molecular packing structure view down (100) plane in crystal **1**. (e) Crystal index and energy frameworks of crystal **1**. (red dash lines: hydrogen bonds, blue dash line: π···π interaction, gray arrows: layer expansion or contraction when crystal bending, gray dash line arrows: molecular moving directions when twisting crystals).

2.5 Optical waveguiding properties

Taking advantage of the integrated elastic-bending and plastic-twisting deformations as well as acidichormic behaviors of crystal **1**, Crystalline optical waveguides with flexible and color-tunable properties were prepared. The optical waveguide tests of crystal **1** were carried out in the straight, bent, twisted and straight (T-straight), and twisted and bent (T-bent) states. The twisted crystal employed in these measurements was deformed with 6 pitches within 5.0 mm length (See Supporting Information Figure S18 for detailed experimental procedures). Although some slightly twisted crystalline optical waveguides have been reported [40] previously, severely twisted crystals generally have an extremely poor light transducing ability due to the light leak from the crystal body. The photographic images of those samples irradiated by a 355 nm laser beam at different positions of crystal **1** are shown in Figure 5a–d. The excited spot was scanned from the left side to the right side of a crystal with an interval length of 1.0 mm, and the output signals were recorded on the left side (white dash circles). When the laser beam moved away from the left tip, the recorded emission intensity decreased in all the measurements (Figure 5g). By fitting the data in Figure 5g, the optical loss coefficient (OLC), a crucial parameter to evaluate optical transducing capability calculated by a reported method, [37,40] has been determined to be 0.120, 0.155, 0.226 and 0.237 dB / mm for the straight, bent, T-straight and T-bent crystals, respectively (Figure 5h). These values are comparable

to those of other flexible crystalline optical waveguides (Supporting Information Table S3). Compared with the straight crystal, the bent and twisted crystals show higher OLCs, demonstrating that deformations degrade optical transmission ability. The optical waveguide tests of crystal **1@H** were carried out in the straight states. Compared with the crystal **1** straight crystal, the crystal **1@H** show higher OLCs, demonstrating that acidichromic degrade optical transmission ability (Supporting Information Figure S19). Then the stability of crystal **1** placed for a week is tested. The optical loss coefficient of the sample are similar to that of the original crystal **1**, indicating excellent robustness (Supporting Information Figure S20). Then, the optical waveguide of **1//1@H** was tested by the aforementioned method to realize the purpose of flexible and adjustable optical signals on a single crystal. A heterojunction sample **1//1@H** with a third of the length fumed in HCl vapor for **1** minute was prepared. The sample **1//1@H** was gradually excited from the original tip to the protonated tip, and the emission spectra were recorded at the original tip simultaneously (Figure 5e). As shown in Figure 5i, the output signals remained a constant green emission (from **1** only, 544 nm) in the first three tests, then changed into a dual-band yellow emission (from **1** and **1@H**, 545 and 583 nm), and finally a single band red emission (from **1@H** only, 631 nm). The CIE coordinates of the optical waveguide outputs as plotted in Figure 5k localize in the region of green, yellow and deep red. The sample was further twisted 180° and the signal was excited and collected from the other end (the protonated part) of the twisted crystal **1//1@H** (Figure 5f). Reasonably, the output signals switched from deep red (652 nm), yellow (643 and 598 nm), and green emission (545 nm)) (Figure 5j). To our knowledge, this is the first optical tuner of crystalline optical waveguides that combines flexibility, acidchromism and optical transmission, and we envisage applications in optoelectronics for information integration or encryption.

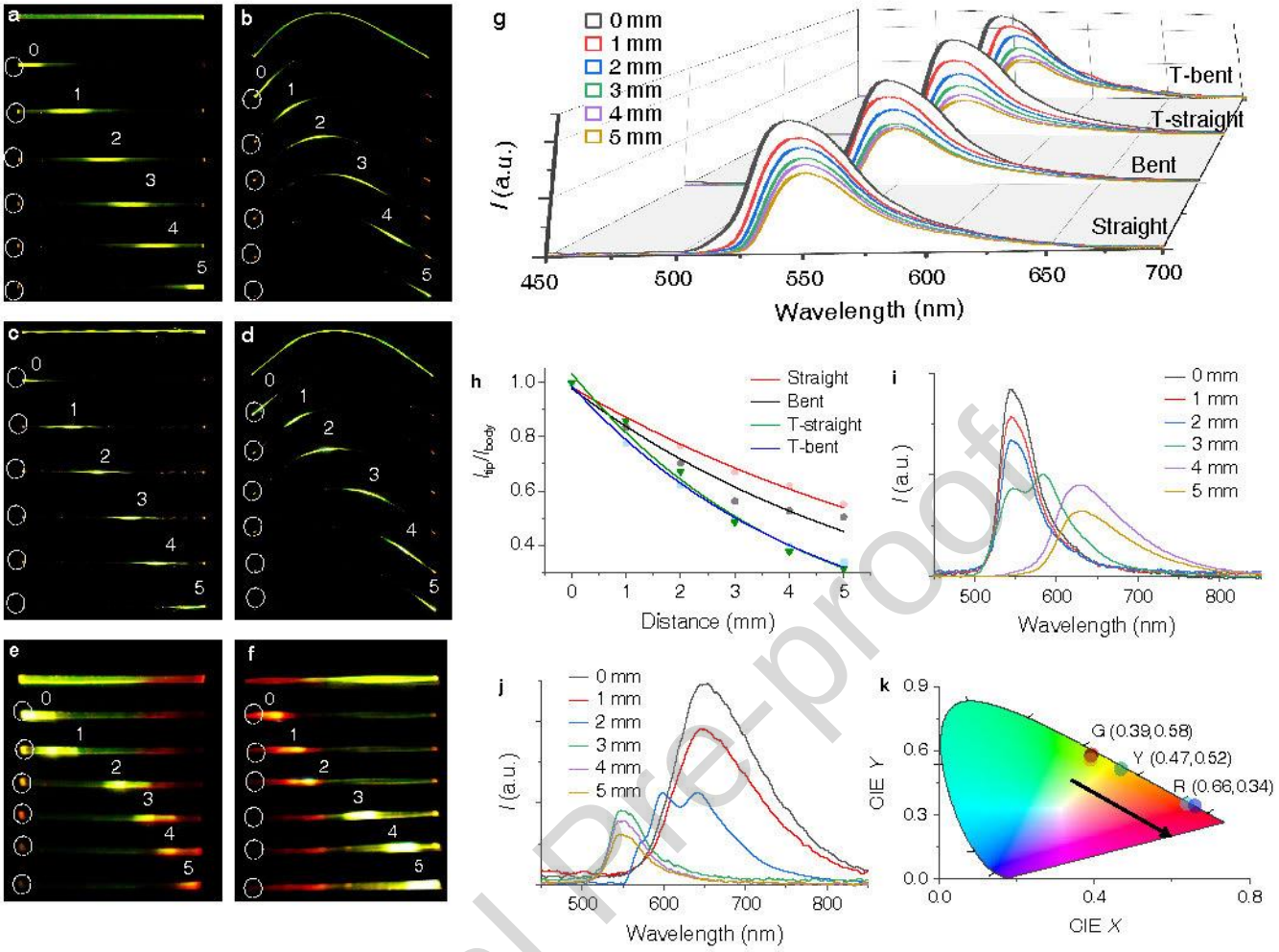

Figure 5 | (a–d) Fluorescence photographs of straight (a), bent (b), twisted (c) and twisted and bent (d) crystals excited with a UV lamp (uppermost line) and with 355 laser focused at different positions. (e, f) Fluorescence photographs of a partly protonated crystal with a UV lamp (uppermost line) and with a 355 nm laser focused at different positions started from neutral (e) and protonated (f) sides. (g, h) Fluorescence spectra (g) collected at a tip (white dash circle) and I_{tip} / I_{body} decays (h) of single crystals (length = 5.0 mm) in the straight, bent, twisted, and twisted and bent states at room temperature. (i–k) Fluorescence spectra collected at a tip (white dash cycle) upon exciting started from neutral (i) of **1//1@H** and protonated (j) side of twisted **1//1@H**. CIE coordinates (k) of the emission spectra shown in panel i.

3. Conclusions and Outlook

In summary, a Schiff base compound **1** was prepared in this work for the purpose of designing organic crystals that combine multi-type flexibilities and optical output tunability. The well-designed crystals **1** display excellent bending elasticity and twisting plasticity which can be independently controlled. Notably, various heterojunction structures of **1//1@H**, **1//1@H//1** and **1@H//1//1@H** by partly acid-fuming of slender crystals display an erasing-rewriting feature, enabling the regulation of emission outputs to be reconfigurable. The excellent mechanical properties of the crystals and the acidichromism are compatible with each other. Furthermore, taking advantage of the integrated deformations and acidichromic property, we have successfully constructed active crystalline optical waveguides with high transduce-pathway

deformability and wide-range output tunability. The results provide a feasible strategy for quickly and easily regulating the output signals of flexible crystalline optical waveguides, and pave the way for the application of organic-based molecular crystalline materials in future flexible intelligent optoelectronic and wearable electronic devices.

Acknowledgments

This work was supported by the National Natural Science Foundation of China (52173164, 52373181) and the Natural Science Foundation of Jilin Province (20230101038JC).

Author Contributions

Xiuhong Pan did the experiments, analysis, validated the results, and wrote the manuscript. Qi Di contributed to the theoretical calculation. Xuesong Yang and Linfeng Lan contributed to material synthesis and mechanical properties. Hongyu Zhang provided key advice, supervised the study and funding acquisition.

Declaration of Interests

There are no conflicts to declare.

References

[1] Z. Wu, Y. Wang, X. Liu, C. Lv, Y. Li, D. Wei, Z. Liu, Carbon-Nanomaterial-Based Flexible Batteries for Wearable Electronic, Adv. Mater. 31 (2019) 1800716.
[2] C. Y. Wang, K. L. Xia, H. M. Wang, X. P. Liang, Z. Yin, Y. Y. Zhang, Advanced Carbon for Flexible and Wearable Electronics, Adv. Mater. 31 (2019) 1801072.
[3] H. Park, S. Kim, J. Lee, I. Lee, S. Bontapalle, Y. Na, K. Sim, Organic flexible electronics with closed-loop recycling for sustainable wearable technology, Nat. Electron. **7** (2024) 39–50.
[4] L. Lan, L. Li, J. Qi, X. Pan, Q. Di, P. Naumov, H. Zhang, Woven organic crystals, Nat. Commun. 14 (2023) 7582.
[5]. Y. Wang, L. Sun, C. Wang, F. Yang, X. Ren, X. Zhang, H. Dong, W. Hu, Organic crystalline materials in flexible electronics, Chem. Soc. Rev. 48 (2019) 1492–1530.
[6] B. Fraboni, A. Fraleoni-Morgera, Y. Geerts, A. Morpurgo, V. Podzorov, Organic Single Crystals: An Essential Step to New Physics and Higher Performances of Optoelectronic Devices, Adv. Funct. Mater. 26 (2016) 2229–2232.
[7] S. Ghosh, M. K. Mishra, S. B. Kadambi, U. Ramamurty, G. R. Desiraju, Designing Elastic Organic Crystals: Highly Flexible Polyhalogenated N-Benzylideneanilines, Angew. Chem. Int. Ed. 54 (2015) 2674 – 2678.
[8] S. Hayashi, T. Koizumi, Elastic Organic Crystals of a Fluorescent π-Conjugated Molecule, Angew. Chem. Int. Ed. 55 (2016) 2701–2704.
[9] R. Huang, C. Wang, Y. Wang, H. Zhang, Elastic Self-Doping Organic Single Crystals Exhibiting Flexible Optical Waveguide and Amplified Spontaneous Emission, Adv. Mater. 30 (2018) 1800814.
[10] S. Hayashi, S.-y. Yamamoto, D. Takeuchi, Y. Ie, K. Takagi, Creating Elastic Organic Crystals of π-

Conjugated Molecules with Bending Mechanofluorochromism and Flexible Optical Waveguide, Angew. Chem. Int. Ed. 57 (2018) 17002.
[11] Z. Lu, Y. Zhang, H. Liu, K. Ye, W. Liu, H. Zhang, Optical Waveguiding Organic Single Crystals Exhibiting Physical and Chemical Bending Features, Angew. Chem. Int. Ed. 59 (2020) 4299.
[12] W. Wu, K. Chen, X. Zhang, T. Wang, S. Li, H. Zhao, L. Zhou, X. Huang, H. Hao, Organic Crystals with Response to Multiple Stimuli: Mechanical Bending, Acid-Induced Bending and Heating-Induced Jumping, Chem. Eur. J. 29 (2023) e202202598.
[13] J. Peng, J. Zhao, K. Ye, H. Gao, J. Sun, R. Lu, Light-Induced Bending of Needle-Like Crystals of Naphthylvinylbenzoxazole Triggered by trans–cis Isomerization, Chem. Asian J. 13 (2018) 1719–1724.
[14] A. Hirano, T. Hashimoto, D. Kitagawa, K. Kono, S. Kobatake, Dependence of Photoinduced Bending Behavior of Diarylethene Crystals on Ultraviolet Irradiation Power, Cryst. Growth Des. 17 (2017) 4819–4825.
[15] Ž. Skoko, S. Zamir, P. Naumov, J. Bernstein, The Thermosalient Phenomenon. "Jumping Crystals" and Crystal Chemistry of the Anticholinergic Agent Oxitropium Bromide, J. Am. Chem. Soc. 132 (2010) 14191–14202.
[16] S. Ghosh, C. M. Reddy, Elastic and Bendable Caffeine Cocrystals: Implications for the Design of Flexible Organic Materials, Angew. Chem. Int. Ed. 51(2012) 10319–10323.
[17] M. Annadhasan, D. P. Karothu, R. Chinnasamy, L. Catalano, E. Ahmed, S. Ghosh, P. Naumov, R. Chandrasekar, Micromanipulation of Mechanically Compliant Organic Single-Crystal Optical Microwaveguides, Angew. Chem. Int. Ed.59 (2020) 13821.
[18] M. Annadhasan, A. R. Agrawal, S. Bhunia, V. V. Pradeep, S. S. Zade, C. M. Reddy, R. Chandrasekar, Mechanophotonics: Flexible Single-Crystal Organic Waveguides and Circuits, Angew. Chem. Int. Ed. 59 (2020) 13852.
[19] T. Kim, M. K. Al-Muhanna, S. D. Al-Suwaidan, R. O. Al-Kaysi, C. J. Bardeen, Photoinduced Curling of Organic Molecular Crystal Nanowires, Angew. Chem. Int. Ed. 52 (2013) 6889 – 6893.
[20] H. Wang, P. Chen, Z. Wu, J. Zhao, J. Sun, R. Lu, Bending, Curling, Rolling, and Salient Behavior of Molecular Crystals Driven by [2+2] Cycloaddition of a Styrylbenzoxazole Derivative, Angew. Chem. Int. Ed. 56 (2017) 9463 – 9467.
[21] H. Liu, Z. Lu, B. Tang, C. Qu, Z. Zhang, H. Zhang, A Flexible Organic Single Crystal with Plastic-Twisting and Elastic-Bending Capabilities and Polarization-Rotation Function, Angew. Chem. Int. Ed. 59 (2020) 12944–12950.
[22] S. Saha, G. R. Desiraju, A hand-twisted helical crystal based solely on hydrogen bonding, Chem. Commun. 53 (2017) 6371–6374.
[23] S. Saha, G. R. Desiraju, Crystal Engineering of Hand-Twisted Helical Crystals, J. Am. Chem. Soc. 139 (2017) 1975–1983.
[24] T. Takeda, M. Ozawa, T. Akutagawa, Jumping Crystal of a Hydrogen-Bonded Organic Framework Induced by the Collective Molecular Motion of a Twisted π System, Angew. Chem. Int. Ed. 58 (2019) 10345–10352.
[25] P. Naumov, S. C. Sahoo, B. A. Zakharov, E. V. Boldyreva, Dynamic Single Crystals: Kinematic Analysis of Photoinduced Crystal Jumping (The Photosalient Effect), Angew. Chem. Int. Ed. 52 (2013) 9990–9995.
[26] Q. Di, J. Li, Z. Zhang, X. Yu, B. Tang, H. Zhang, H. Zhang, Quantifiable stretching-induced fluorescence shifts of an elastically bendable and plastically twistable organic crystal, Chem. Sci. 12 (2021) 15423–15428.

[27] R. Samanta, D. Kitagawa, A. Mondal, M. Bhattacharya, M. Annadhasan, S. Mondal, R. Chandrasekar, S. Kobatake, C. M. Reddy, Mechanical Actuation and Patterning of Rewritable Crystalline Monomer−Polymer Heterostructures via Topochemical Polymerization in a Dual-Responsive Photochromic Organic Material, ACS Appl. Mater. Interfaces. 12 (2020) 16856–16863.
[28] Z. Jiang, H. Zhao, W. Wu, K. Chen, H. Yu, T. Wang, X. Huang, N. Wang, L. Zhou, H. Hao, Multi-stimuli responsive organic polymorphic crystals: anisotropic elasticity and plasticity, mechanochromism and photomechanical motions, J. Mater. Chem. C. 11 (2023) 4375-4383.
[29] S. Bhandary, A. J. Thompson, J. C. McMurtrie, J. K. Clegg, P. Ghosh, S. R. N. K. Mangalampalli, S. Takamizawa, D. Chopra, The mechanism of bending in a plastically flexible crystal. Chem. Commun. 56 (2020) 12841-12844.
[30] L. Lan, L. Li, Q. Di, X. Yang, X. Liu, P. Naumov, H. Zhang, Organic Single-Crystal Actuators and Waveguides that Operate at Low Temperatures. Adv. Mater. 34 (2022) 2200471.
[31] L. Lan, X. Yang, B. Tang, X. Yu, X. Liu, L. Li, P. Naumov, H. Zhang, Hybrid Elastic Organic Crystals that Respond to Aerial Humidity. Angew. Chem. Int. Ed. 61 (2022) e202200196
[32] X. Chu, Z. Lu, B. Tang, B. Liu, K. Ye, H. Zhang, Engineering Mechanical Compliance of an Organic Compound toward Flexible Crystal Lasing Media. J. Phys. Chem. Lett. 11 (2020) 5433–5438.
[33] D. P. Karothu, G. Dushaq, E. Ahmed, L. Catalano, M. Rasras, P. Naumov, Multifunctional Deformable Organic Semiconductor Single Crystals, Angew. Chem. Int. Ed. 60 (2021) 26151.
[34] B. Tang, X. Yu, K. Ye, H. Zhang, Manifold Mechanical Deformations of Organic Crystals with Optical Waveguiding and Polarization Rotation Functions, Adv. Opt. Mater. 10 (2022) 2101335.
[35] L. Lan, Q. Di, L. Li, B. Liu, X. Yu, P. Naumov, H. Zhang, Packing-Dependent Mechanical Properties of Schiff Base Crystals, Cryst. Growth Des. 22 (2022) 3435–3441.
[36] H. Liu, K. Ye, Z. Zhang, H. Zhang, An Organic Crystal with High Elasticity at an Ultra-Low Temperature (77 K) and Shapeability at High Temperatures, Angew. Chem. Int. Ed. 58 (2019) 19081.
[37] H. Liu, Z. Lu, Z. Zhang, Y. Wang, H. Zhang, Highly Elastic Organic Crystals for Flexible Optical Waveguides, Angew. Chem. Int. Ed. 57 (2018) 8448.
[38] O. V. Dolomanov, L. J. Bourhis, R. J. Gilde, J. A. K. Howard, H. Puschmann, OLEX2: a complete structure solution, refinement and analysis program, J. Appl. Cryst. *42* (2009) 339–341.
[39] M. J. Turner, J. J. McKinnon, S. K. Wolff, D. J. Grimwood, P. R. Spackman, D. Jayatilaka, M. A. Spackman, CrystalExplorer17, University of Western Australia, Perth, 2017.
[40] B. Tang, M. Li, X. Yu, H. Zhang, Achieving two things at one stroke: crystal engineering simultaneously optimizes the emission and mechanical compliance of organic crystals, J. Mater. Chem. C, 10 (2022) 3894–3900.

Graphical abstract